Effect of polymer-coated silica particles in a Portland cement matrix via in-situ infrared spectroscopy

Tahereh Mohammadi Hafshejani[1,*], Chao Feng[1,2,*], Jonas Wohlgemuth[1], Felix Krause[1], Andreas Bogner[3], Frank Dehn[3] and Peter Thissen[1]

Abstract

It is often of great importance in engineering to know precisely the properties of a material used with regard to its strength, its plasticity or its brittleness, its elasticity, and some other properties. For this purpose, material samples are tested in a tensile test by clamping the sample with a known starting cross-section in a tensile testing machine and loading it with a tensile force F. The force is then graphically displayed over the length change ΔL caused. This curve is called the force-extension diagram. In this study, a new measurement method enables for the first time, depending on the applied uniaxial stress, an insight at the atomic level into various energy dissipation processes at cement-based materials with the help of infrared spectroscopy. The samples are modified by adding SiO_2 particles, which are coated by a polymer (PEG-MDI-DMPA) of different PEG molecular weights. Results show that elongating and breakage of $Si-O-Si$ and $C-O$ bonds play an essential role in the strain energy dissipation. Compared to the pure cement, the modified samples are affected more by elongating and breakage of $Si-O-Si$, as the admixture can effectively reduce the energy barrier of the hydrolytic reaction. The incorporating of particles into the cement matrix induces new mechanisms for energy dissipation by stretching of $O-Si-O$ bending vibrations. Stretching vibration of the $O-H$ group indicates that part of the energy is dissipated by breakage of hydrogen bonding between the carboxyl group and PEG chains. Besides, a higher value of the ultimate fracture force following an increase in the molecular weight of PEG shows stronger bonding between particles and the cement matrix. As the chain-length of PEG is increased, less energy is absorbed through the other processes (especially at a higher level of strain). Thus, there is a balance between the whole deformation (toughness) and the strength of samples with the increase of the PEG molecular weight.

Keywords

Cement matrix, shape memory polymers, SiO_2 particles, energy dissipation, in-situ IR spectroscopy

Introduction

Many infrastructural facilities like dams, road foundations, bridges, tunnels and others are constructed of concrete. Due to impact loading or the dynamic shock of moving vehicles, earthquakes, etc., some of these concrete structures are affected by vibration forces, resulting in damage and fatigue accumulations of structure.[1,2] Structure type and applied dynamic load are two factors that change the amplitude and frequencies of the induced vibration in a given structure. In this regard, vibrational control is essential to prolong the life of the structure and reduce economic cost. [3,4] Damping, dissipation of energy in the materials

Corresponding author:
Peter Thissen, Karlsruher Institut für Technologie, Institut für Funktionelle Grenzflachen, Hermann von Helmholtz Platz 1, 76344 Eggenstein-Leopoldshafen, Deutschland.
Email: peter.thissen@kit.edu

under load, is one the best method to alleviate the dynamic vibrations.

Mechanical energy dissipation is the transformation of energy into another form of energy such as heat.[5] There are two approaches for a vibration to be damped: passive damping and active damping. In active damping a sensor and actuator are required to overcome the vibration, which is efficient but expensive. In passive damping (cheap and more prevalent way), some kinds of materials are used which can dissipate the energy of vibration and are able to convert it to heat.[5] Some notable advantages of dissipation are noise reduction, longer service life, better control and also improved resistance to mechanical perils.

Polymers are widely used in passive damping to reduce the vibration of dynamic stresses and increase system performance.[6 8] Constantinides at el., characterized the ability of polyethylene (PE) and polypropylene (PP) to resist impact deformation and dissipate impact energy.[9] Finegan and Gibson[10] investigated the damping behavior of polymer composites with coated fibers, reporting that the use of a viscoelastic polymer coating on the fiber is an effective way to improve the damping properties. Furthermore, shape memory polymers are categorized as smart materials that can respond to external sources such as heat, sound and light.[11,12] During this reversible transition, the long range molecular reordering affects the dissipation of the vibration energy.[7] So, we aimed to use a series of polyurethane named PEG-MDI-DMPA (polyethylene glycol - 4,4-diphenylmethane diisocyanate - and dimethylolpropionic acid) which are known as a triple shape memory polymer.[13] In recent years, a new class of materials, having core/shell structures, are made by depositing a secondary material (shell) onto core nanoparticles.[14,15] These hybrids can combine the advantages of core particles and organic polymers.[16] Gao et al. showed that SiO_2 nanoparticles grafted by rubbery block copolymer increased the ductility, fracture toughness and fatigue crack growth resistance of the epoxy matrix.[17] Jiang et al. suggested, using silica nanoparticles that attached to graphene oxide into epoxy to enhance the mechanical properties of the composites.[18] Han et al.[19] showed that incorporation of 1–5 wt% TiO_2@SiO_2 particles into concrete improved the compressive and flexural tensile strength by 1.78–5.44% and 55.91–83.30%, respectively, at 3 days. The core/shell materials have been created and developed since early 21st century, however, the idea of using these materials as construction materials was suggested in 2017.[14]

This article is intended to understand the energy dissipation mechanisms in SiO_2@polymer–matrix composites for evaluating the samples damping behavior. The study is regarded to use in-situ infrared spectroscopy combined with our self-made mechanical instrument (Bieger) in order to apply the dynamic loads and IR radiation simultaneously. It is supposed that the obtained IR spectra can provide us useful information about how modified samples react to mechanical loading and, as well, their mechanism in energy dissipation. Figure 1 indicates the predicted effect of particles in inhibiting crack propagation and increasing energy dissipation of hardened cement paste.

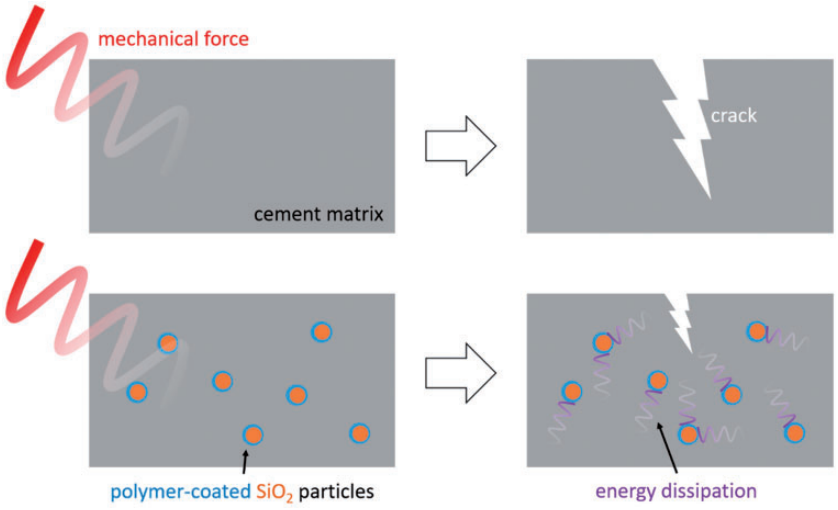

Figure 1. Schematic illustration of the effect of the particles on crack growth. It is assumed that in the pure hardened cement paste, after applying mechanical force fast crack propagation happened which lead to lower fracture force and suddenly release of mechanical force. However, incorporated particles are expected to be barrier against crack growth, resulting in creation of new microcracks which need energy to grow and pass the particles. Consequently, more energy might be dissipated.

Experimental

Chemicals

The SiO_2 powders (Silica gel 60, 0.03-0.2 mm) and Polyethylen glycol 1500 (PEG-1500) were purchased from Carl Roth GmbH & Co. KG, Germany. The Polyethylene glycol 600 (PEG-600), Diphenylmethane 4,4′-diisocyanate (MDI) and Sodium hydroxide solution (NaOH solution, 1 mol/L) were purchased from Merck KGaA, Germany. The 2,2-Bis(hydroxymethyl)-propionic acid (DMPA) was provided from Alfa Aesar, Germany. Portland cement (CEM-I 32.5 R) was supplied by HeidelbergCement AG, Germany.

polymer coated particles and cement-based composites

In this work, 0.015 mol PEG (PEG was PEG-600 and PEG-1500) and 0.012 mol DMPA were dissolved in 200 mL acetone, 9 g SiO_2 powders were added and dispersed by magnetic stirring for 10 min. After that, 0.025 mol MDI in 50 mL of acetone was added dropwise into above dispersion solution under a 750 r/min speed magnetic stirring, this mixture was heated to 75°C and reacted for 6 h under nitrogen protection. The products were filtrated and washed with acetone and deionized water. To improve the dispersity of the particles, the products were treated with NaOH solution for 30 min, then were filtrated again and washed with deionized water until the pH was 7. Polymer coated particles were obtained after 6 h of drying in oven at 50°C.

The cement-based samples were prepared by first mixing the cement and each type of particles (with PEG-600 and PEG-1500), this mixture was stirred mechanically for 1 min. And then, under continuous stirring, water was added and the resulting mixture was mixed finally for 2 min. And there was also a control sample without particles. For all of the samples,the water/cement ratio was 0.4 while the particle/cement ratio was 0.07. As the difference in modified samples comes from the molecular weight of PEG, the specimens are coded as PEG-i-C (i= molecular weight of PEG and C denoted the Cement matrix). Composition of three groups of pastes is shown in Table 1.

Table 1. Detailed information of mixture compositions.

Powder phase	Particle/ cement	Water/ cement	Aging time
Pure cement	0	0.4	28 days
PEG 600 C	0.07	0.4	28 days
PEG 1500 C	0.07	0.4	28 days

Due to declining the IR beam scattering, EcoMet 250 pro (Buehler) polisher was used to polish the cement-based materials. Micro polish aluminum oxide powder (alumina) was used at very fine grain size, as with 0.05 μm. The base-speed was 150 rpm, the load was 4 lbs and the polishing time was 2:00 minutes. Then, the polished specimens were cut, by means of IsoMet 1000 Precision Saw (Buehler) instrument, into rectangular samples with the size of $30 \times 10 \times 0.5$ mm which is the required dimension for being used in our self-made mechanical device.

Fourier-Transform infrared spectroscopy (FTIR) combined with a three-point bending test. FTIR measurement (spectra from 400 to 4000 cm^{-1}, reflection mode), by VERTEX 70, and applying force in different positions was done simultaneously. In order to apply force on the samples, our self-made device (Bieger); placed into an N_2-purged glovebox; was used.

An introduction to Bieger and its performance. The Bieger consists of a movable sample holder which is colored in black (Figure 2(a), No. 1) moving towards a nose-like metal piece (Figure 2(a), No. 4). The sample is placed inside the slot, which is located in sample holder (Figure 2(a), No. 3). The movable sample holder and the nose-like metal piece are connected through an open current circuit. As soon as the sample meets the nose-like metal piece for the first time, the current circuit is closed and defined as zero position. It is worth mentioning that a full rotation of the stepper motor includes 51200 equal steps. Each step in motor results in spindle rotation and hence implying movable sample holder downwards. After a full rotation of stepper motor, the movable sample holder goes down as 0.75 mm. The number of steps and the value of deflections have been set with the help of the software, written in LABVIEW.

After the sample comes to zero position, the steps were increased; for instance, the spindle turns 200 steps, equal to 2.9 μm downward movement (the value of deflection). Then, in this position FTIR measurement is started. After performing the FTIR, the sample moves back to the zero position and the next FTIR test is performed. As a next position, the spindle is turned 400 steps, equal to 5.8 μm (the whole procedure is shown in Figure 2(c)). This process is repeated and stopped via a computer-based program controlling the movable sample holder movement. It is important to notice that the point of reflection (top of the moment of inertia of the sample) does never change during the bending load of the sample.

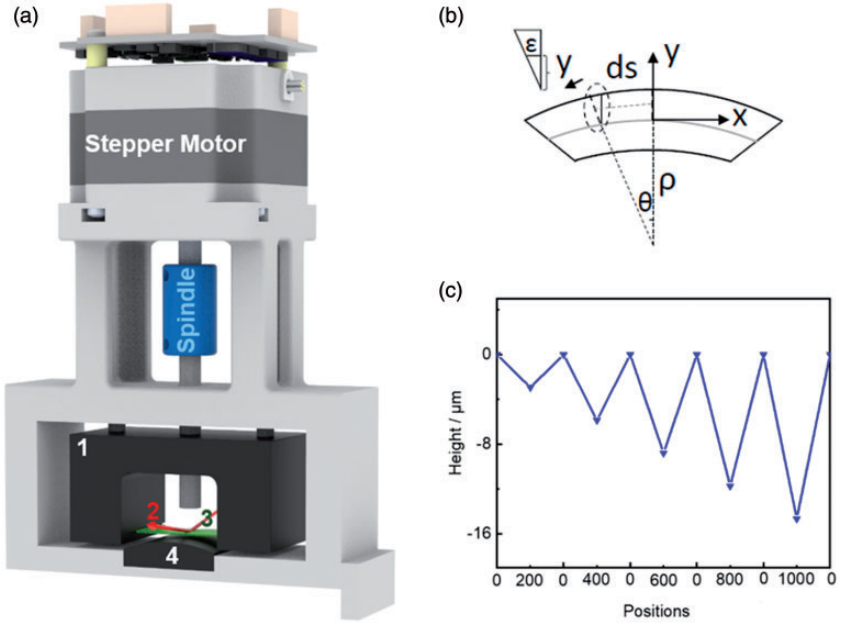

Figure 2. The schematic illustration of the self made instrument (a) contain stepper motor and spindle (loading force parts) as well as 1 movable sample holder, 2 IR beam, 3 sample and 4 nose like metal piece. (b) Schematic illustration of the relation between the radius of curvature, ρ, wafer curvature and the strains within a wafer exposed to bending moments. (c) The graph shows the procedure of applying loading on the sample in different positions (the number of positions is equal to the number of spindle steps).

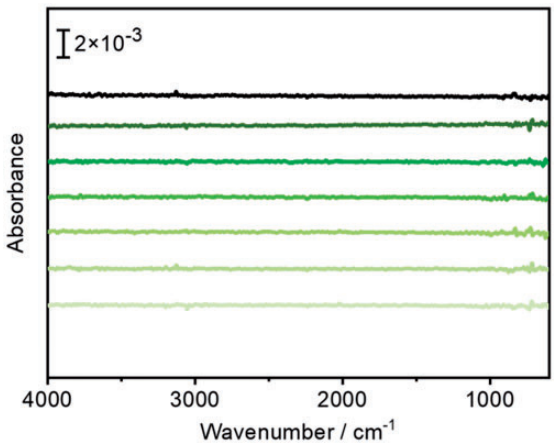

Figure 3. FTIR spectra of repeated measurements on gold coated aluminum which was bended equal to 2.9 μm more in each step.

To prove this fact, several measurements of gold-coated aluminum samples which showed complete reflectivity were carried out while the deflection was increased by 2.9 μm each time. The results are presented in Figure 3.

The curvature is calculated in reference to the previous report from the following equation

$$\rho = \frac{x^2}{8d} \tag{1}$$

where x is the sample length (30 mm) and d is deflection (μm) value in each position.[20]

We use the Euler approximation to associate the bending moment with the deflection of the samples; ($\theta = \frac{\varepsilon}{y} = \frac{1}{\rho}$, $\rho d\theta = ds$, $\frac{dy}{dx} = tan\theta$, Figure 2). And as a result, the below formula is acquired in order to force, stress and strain calculation.

$$\frac{\varepsilon}{d} = \frac{1}{\rho} = \frac{Fx}{2EI} \tag{2}$$

$$Moment\ of\ inertia: \quad I = \frac{bh^3}{12}$$

So the strain formula is as

$$\varepsilon = \frac{6Fxd}{Ebh^3} \tag{3}$$

By applying Hooke's law, and incorporating equation (3), the stress can be expressed as,

$$\sigma = \frac{6Fxd}{bh^3} \tag{4}$$

where E is Young's modulus of Si (165 GPa),[21] ρ the radius of curvature in each position (mm), F applied force (GPa mm^2), d deflection (μm) and ε strain. I is

called the moment of inertia ($I = \frac{bh^3}{12}$, where b and h are width and thickness of the sample, respectively).

Scanning electron microscope (SEM) analysis

Surface morphology of samples before and after bending was analyzed by Scanning Electron microscopy using Philips XL30 ESEM-FEG (Firma, Ort, Land) at 20 kV.

Nanoindentation investigation

Proper surface preparation is crucial for nanoindentation analysis and therefore great care has been taken. Cross-sections of the specimens were cut using a Buehler IsoMet 1000 diamond saw (Buehler, Lake Bluff, Illinois, USA). After expoxy-mounting three consecutive grinding steps followed by three consecutive polishing steps using a Buehler EcoMet 250 Pro Grinder Polisher were performed. In the last step a 50 nm alumina powder has been utilized. Each polishing step was followed by 3 min of ultrasonication in water with detergent to remove any loose particles.

Nanoindentation was performed using an Ultra Nanoindentation Tester UNHT^3 (Anton Paar GmbH, Graz, Austria) equipped with a diamond Berkovich tip. For each specimen a quadratic grid of 289 indents with a spacing of 10 µm between indents both in x and y direction was collected at a representative area. The applied load was increased for 10 s until the maximum load of 2 mN was reached and held for 5 s, followed by a 10 s unloading period. Young's modulus was then calculated using the Oliver and Pharr method.[22,23]

Since the diameter of the indents is only about 3 µm, different phases of the hardened cement paste with different Young's moduli were analyzed per specimen. Therefore, the standard deviation is large if only the average of all these phases is given. Nevertheless, these values contain information about the average material properties.

Results and discussion

Synthesis and characterization

The PEG-MDI-DMPA solution is synthesized through polymerization using poly ethylene glycol (PEG) with two molecular weights, 600 g mol ^{1} and 1500 g mol ^{1}, diphenylmethane diisocyanate (MDI) and dimethylolpropionic acid (DMPA). The chemical structure of the synthetic polymer is shown in Figure 4.

According to IR results in Figure 5 (red line), the designed polymer is successfully synthesized. It is

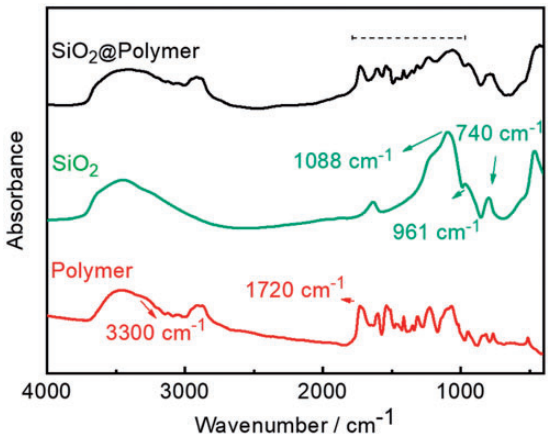

Figure 5. IR curves of synthetic polymer, SiO_2 particles and polymer coated SiO_2 particles (SiO_2@polymer).

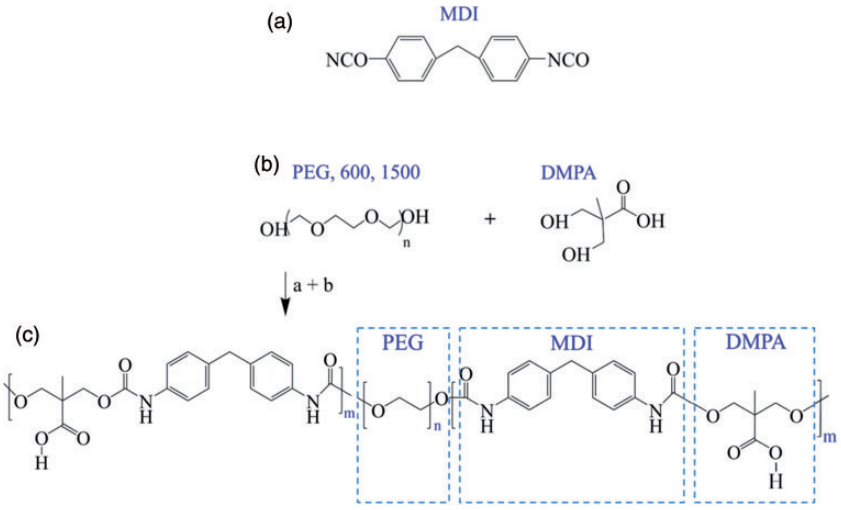

Figure 4. Synthetic process of PEG MDI DMPA.[24]

reported that the stretching vibration of isocyanate ($-N=C=O$) appears around 2270 cm ^{1}.[13] As shown, there is no peak at mentioned wavenumber, indicating the MDI completely reacted. The peaks observed around 3300 cm ^{1} and 1720 cm ^{1} are related to the stretching vibration of $N-H$ and $C=O$, respectively, illustrating the formation of the urethane group ($-NHCOO-$). [13,24]

The green IR curve shows the range of the wavenumber region for SiO_2 particles; the stretching vibration of the $Si-O-Si$ bond appears at 1088 cm ^{1}, 961 cm ^{1}, and 740 cm ^{1}. In addition, the peak around 461 cm ^{1} is associated with the bending vibration of $O-Si-O$.[25] The determined range (black line) confirms that it is not straightforward to show if the SiO_2 and polymer are physically or chemically bound together. There is no obvious additional peak that shows the creation of chemical interaction such as $Si-O-C$. However, the peak assignment at 1000-1500 cm ^{1} is difficult because of contributions from several species, including $Si-O-Si$ and $Si-O-C$ vibrations.[26]

Figure 6 shows the SEM images of the SiO_2 particles without (a) and with (b) polymer coating. As illustrated, the polymer is thickly grafted to the particles.

Figure 7 depicted the microstructure morphologies of hardened cement samples before modification ((a, b)) and after incorporation of particles ((c, d)) cured up 28 days. As shown in Figure 7(b), C-S-H is obvious hydrate phase in the pure cement sample which is observed as condensed phase. The homogenous distribution of particles is shown in Figure 7(c). Lu et al. [27] revealed that adding particles will generate lots of pores, which would prevent from the micro

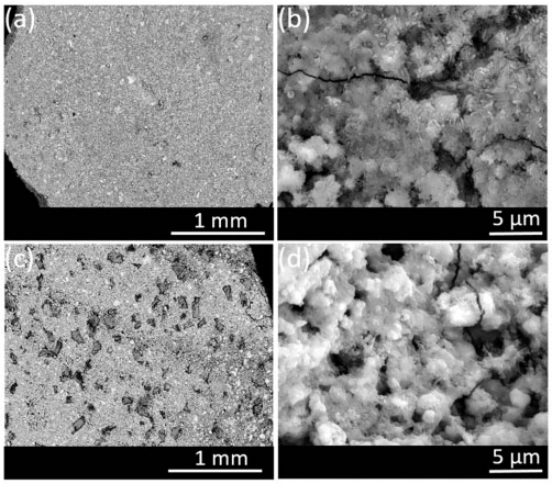

Figure 7. SEM images of 28 days pastes morphology (a, b): sample without particles and (b, d): uniform distribution of particles (SiO_2@polymer) in cement matrix.

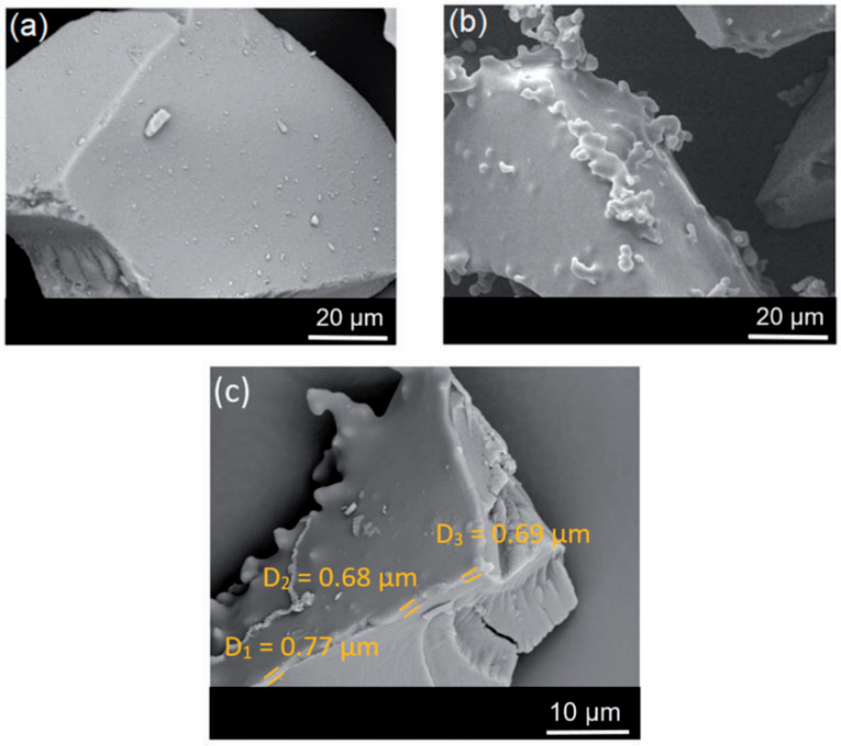

Figure 6. SEM images of (a): SiO_2 without polymer coating and (b): SiO_2@ polymer, the diameter of the inorganic core is between 50 –100 microns and the thickness of the polymer coating is between 0.5 – 5 microns (c).

cracks growth (increasing mechanical strength).[28] Consequently, more cracks will be produced in the matrix to dissipate the external energy. However, in their study, the particles within the specimens were not perfectly distributed. Kamrani et al.[29] reported that uniformly distributed nanoparticles enhance the elastic modulus of the composite by behaving like a homogenous structure and resisting the plastic deformation at lower stress. Also, Slipenyuk et al. indicated, a boundary between agglomerated particles does not transfer tensile and shear stress.[30] Therefore, it is well known that the amount of homogeneous distribution of reinforcement particle strongly influences the mechanical properties. When the particles are added, the microstructure of the hardened pastes seemed to be dense and the polymer phase act like bridge between voids and cracks (Figure 7(d)).

EDX elemental mapping analysis is performed to further investigate the polymer coated particles and their distribution in matrix (Figure 8). The results indicate that Si is present in the core and polymer is localized in the shell. Good distribution of Si in SiO_2@polymer modified cement paste can be possibly related to the layer of polymer that limited the agglomeration of SiO_2 particles.

The main goal of this study is to investigate the energy properties of cement-based materials during the fracture process. The primary characteristic of concrete deforming and fracturing is energy absorption, which can reflect the dynamic process of micro cracks developing, strength reduction and ultimate fracture.[27] Consequently, by analyzing energy dissipation properties of these materials during the fracture process, the damage properties (such as the crack initiation, propagation, coalescence and interaction) can be effectively reflected. Here, considering the absorption and transformation of IR spectroscopy energy into the molecular vibration, we use the indirect method to study the damping capability of our samples.

IR spectra of samples under mechanical loading in different bending position is illustrated in Figure 9. As reported by many previous studies,[31–33] calcium silicate hydrate phases (C-S-H) form about 60% of the hydration products in the hardened cement paste and have a primary effect on the mechanical properties. Furthermore, the structure of C-S-H consists of stacking $Ca-O$ layers reinforced on both sides by silicate chains. Moreover, the silicate tetrahedra can be presented in the form of dimers, dreierketten or a chain of dreierketten.

From the thermodynamic viewpoint, as the pure C-S-H phase undergoes the tensile process, cause of the activation energy reductions, two hydrolytic reactions are taken place (equations (5) and (6)).[34–36] One is that, considering formula No. 5, the ionic bonds between the Ca and $Si-O$ groups are stretched in the presence of water until they break which leads to formation of $Ca-OH$ and $Si-OH$. Another possibility that can happen is the elongation of the covalent $Si-O-Si$ bond till be broken, and the remaining $Si-O$ and Si would immediately react with water to form two $Si-OH$ (equation (6)).

$$Si-O\cdots Ca \;+\; H_2O \;\rightarrow Si-OH \;+Ca-OH \quad (5)$$

$$Si-O-Si \;+\; H_2O \;\rightarrow Si-OH \;+Si-OH \quad (6)$$

The acquired IR results reveal that only reaction No. 6 occurs which means only the silicate chains of calcium silicate hydrate phase are affected (Figure 8). For the pure cement, the absorption of energy happened by stretching the $C-O$ bond in calcium silicate carbonate phase and $Si-O-Si$ bonds in the C-S-H phase (Figure 9(a)). As the strain goes up, the layer structure of C-S-H and calcium silicate carbonate phases are disturbed. They become less organized, which involves the enhancing break and rearrangements of silicate tetrahedral. The peaks at 1266 cm^{-1} and 1187 cm^{-1} are attributed to the antisymmetric

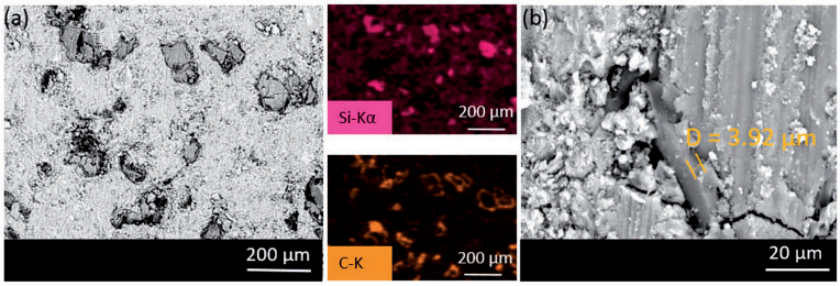

Figure 8. The results of SEM/EDX investigations of the PEG 600 C after 28 days (the images were taken from cross section of sample). Individual elemental maps reveal the presence of silicon related to particles and carbon as cover around them. (b): higher magnification of SEM image which clearly indicates the exitance of organic/inorganic compound in matrix, the measured polymer thickness is 3.92 µm.

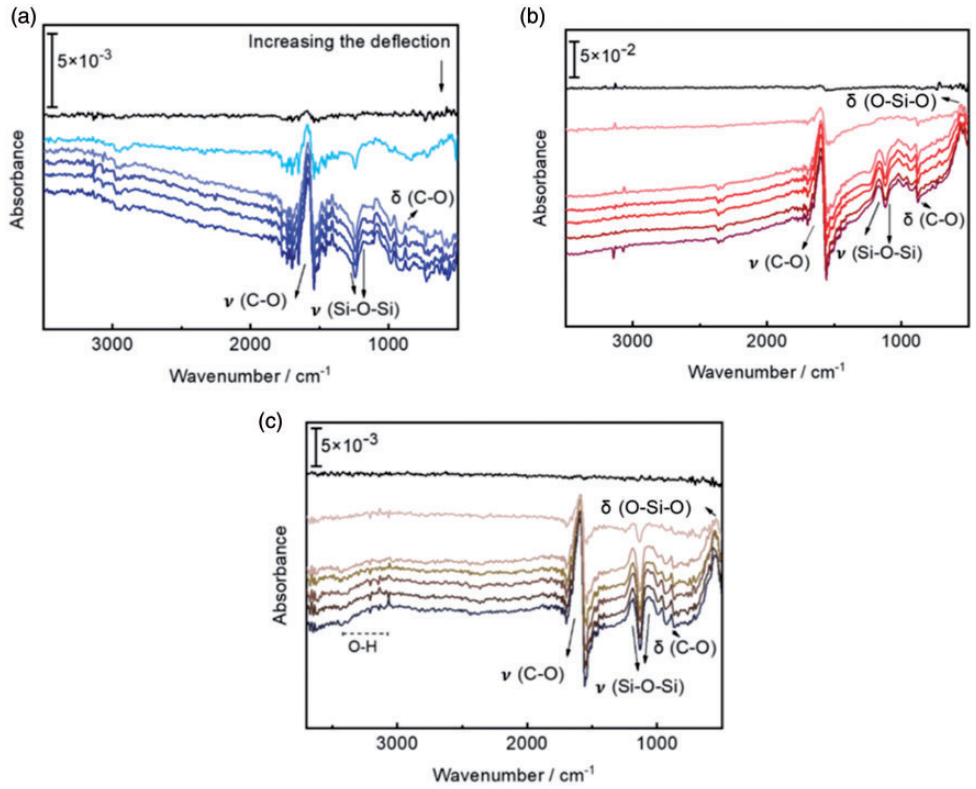

Figure 9. IR spectra of the samples in different bending positions (curvature). (a): un modified cement, (b): PEG 600 C and (c): PEG 1500 C. The black curve in each graph shows the zero position (no curvature). From up to down the value of curvature increases and the last spectra for each sample indicates the max deflection that is supported by samples before complete failure. It is obvious that with increasing the external force, the intensity of observed peaks also enhanced. The observed peaks are indication of different process of energy dissipation in the samples. Two additional peaks (compared to the pure cement) corresponding to bending vibration of *O Si O* and *O H* vibration is found in the modified samples, (b) and (c).

stretching vibration of $Si-O-Si$.[37] The sharp peak at 1582 cm ^{1} and a weak peak at 870 cm ^{1} can be correlated to the asymmetric and bending vibration of the $C-O$ of the CO_3^{2} group presented in the calcium silicate carbonate phase, respectively.[37,38] Since the damage process of the material always starts with the weakest parts, the first mechanism of energy absorption is observed during stretching of $C-O$ bonds.[27]

As it was explained in literature,[39,40] carbonates are formed through different kind of processes. The first mechanism is the diffusion of CO_2 into the empty pores of the surface where it will react with water from the pore solution, forming carbonic acid. Dissociation of carbonic acid leads to the formation of bicarbonate and carbonic ions. Then the reaction between free Ca^{2+} ions and CO_3^{2} results in formation of calcium carbonate. Moreover, carbonate ions can react with calcium ions from the calcium silicate hydrate (C-S-H) phase. The second process will be started by the reaction of CO_2 with the surface oxygen and formation of CO_3^{2} and it will be continued by the reaction between CO_3^{2} and calcium ions. Obviously, carbonate phase grows on cement samples. Since IR measurement is done in reflection mode, it is important that the penetration depth of the IR beam exceeds the always carbonated surface so that sufficient information can be obtained from the bulk sample below. The obtained FTIR results (Figure 9) and the observed differences in the presented peaks indicate that carbonate phase was not a barrier to get the desired information during fracture process.

Regarding the modified hardened cement paste, first of all, the reaction mechanism between particles and the cement matrix should be considered. The kind of interaction between cementitious and polymeric phase is not clear, and this is a controversial issue among researches. Some reported that only physical interaction occurs in the system. Other authors claim for the occurrence of physical and chemical interactions between polymers and Portland cement. Janotka et al.[41] show that chemical interaction can result in the formation of complex structures and changes in the hydrated cement phases morphology, composition and quantity, especially calcium hydroxide can be

Table 2. The obtained values of max deflection (*d*) and max curvature supported by the samples. The value of ultimate force, stress and strain corresponding with max deflection for each sample are also calculated based on the presented formula in experimental part.

Samples	Young's modulus/GPa	Max d/μm	Max curvature/mm	Fracture force/GPa mm^2	Final stress/GPa	Strain
Pure cement	9.18 ± 3.6	199	564.7	8.46E 24	0.0007	0.0002
PEG 600 C	19.2 ± 14.4	583	192.2	5.18E 23	0.027	0.0012
PEG 1500 C	33.9 ± 36.8	509	220.6	8.00E 23	0.066	0.0022

formed. Table 2 shows that the maximum deflection that can be supported by the sample of PEG-600-C is approximately three times as much as for pure hardened cement paste. It appears that these kinds of compounds (with physical or chemical interactions) can make the interlayer region in the modified cement stronger compared to the pure cement. The improvement in mechanical strength of the modified sample is likely because the admixtures can serve as nucleation sites for precipitating cement hydration products, acting like bridge between voids and cracks (Figure 7 (d)); or filler, filling the voids between the cement particles, thus reducing the material porosity.[42]

Figure 10 indicates the intensity of the energy, which is absorbed by different mechanism, as a function of strain. Comparing the stretching vibration intensity of $\boldsymbol{v}$ ($Si-O-Si$) reveals that in the modified cement more $Si-O-Si$ bonds are involved to carry out the strain. As a result, the stress is more distributed and the failure created by strain concentration can be more avoided. This increase in the intensity also indicates that the admixture reduces the energy barrier of the hydrolytic reaction effectively (equation (6)). Presumably, the coordination of carbon from the functional group of the polymers makes Si susceptible to separating from the $Si-O$ group and forming 2 $Si-OH$.[34] Further point is that in the PEG-600-C, the intensity of the $C-O$ bond related to calcium silicate carbonate phase is also enhanced in comparison to the cement without particles (Figure 10). It seems that the carbonate silicate phase in this sample is a weakest phase comparing to the presented phase in pure hardened cement paste. One possibility is that, the particles can decrease the accessibility of Ca^{2+} to connect with carbonate ions, therefore the stretching of $C-O$ bonds existing in carbonate silicate phase of PEG-600-C sample is easier than that of in unmodified cement. As a result, incorporation of particles leads to bearing of more energy with $C-O$ bonds (dissipation of more energy) and also increase the mechanical strength of cement. One highlighted point of the presented IR spectra in Figure 9(b)) is the appearance of the peak around 500 cm^{-1} which is likely emerged as a results of particles incorporation. As it is characterized in the Figure 5 (black FTIR curve), the presented peak around 500 cm^{-1} is due to $O-Si-O$ bending vibrations.[25] The appearance of this peak reveals a new path of energy dissipation in the samples to prevent rapid stress decrease and to postpone the final failure.

The first assumption was that the energy dissipation of particles reinforced cement is mainly contributed to the viscoelastic properties of the polymer phase. Sharafi et al,[7] reported that damping property of polymers is strongly temperature dependent. Elevated damping capability is related to the excessive viscoelastic motion of polymer chains especially around its glass transition temperature. This might be the reason why IR measurements of PEG-600-C showed no peak directly related to the polymeric phase. However, by an increase in the molecular weight of PEG chains (PEG-1500), the broad peak is observed at the wavenumber 3400 cm^{-1}. It is assigned to the $O-H$ vibrations and can be a sign of viscoelastic behavior in the polymer.[13,24] The PEG-MDI-DMPA triple shape memory consists of a soft segment (PEG chains) and a hard segment (MDI-DMPA). The reason for considering PEG as a soft segment is the presence of hydrogen bonding between PEG and the carboxyl group, which obstructs the crystallization of PEG and increases mobility of these chains. MDI and DMPA form the hard segment, and carboxyl groups (presented in hard segment) mainly form the dimers.[24] So, in general there are two types of hydrogen bonding interactions in this polymeric structure: one is formed with themselves as dimers in the hard segment and the other is formed with PEG in the soft segment (Figure 11(a) and (b)).[24]

In this polymer, increasing the molecular weight of PEG means less MDI-DMPA segment content and fewer carboxyl groups. Therefore, one can say, increasing chain-length of PEG might induce more hydrogen bonding between PEG and carboxylic acid. As the stretching vibration of $O-H$ is observed in the sample containing PEG-1500, it is more likely that the corresponding peak is associated with the hydrogen bonding carboxyl groups and soft segment (not between two carboxylic groups). Therefore, part of energy is absorbed to stretch and break the $O-H$

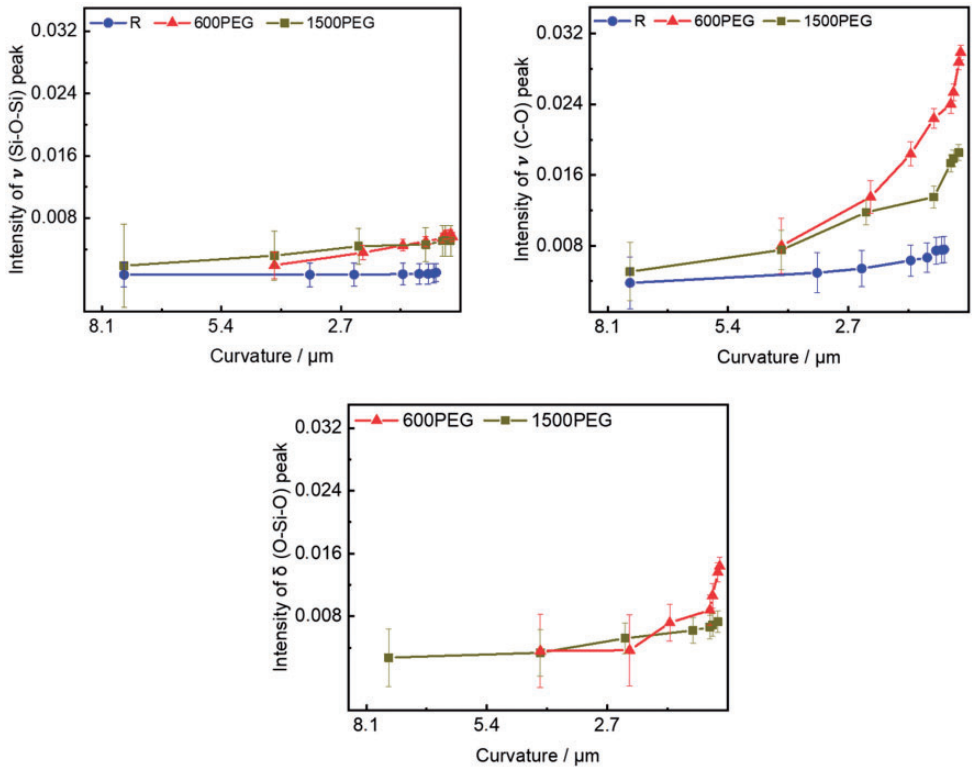

Figure 10. The measured intensity of the stretching vibration of (*Si O Si*), bending vibration of *O Si O* and (*C O*) peaks of the pure cement, PEG 600 C and PEG 1500 C as a function of curvature (μm). Each point represents one bending position when the samples undergo external mechanical force.

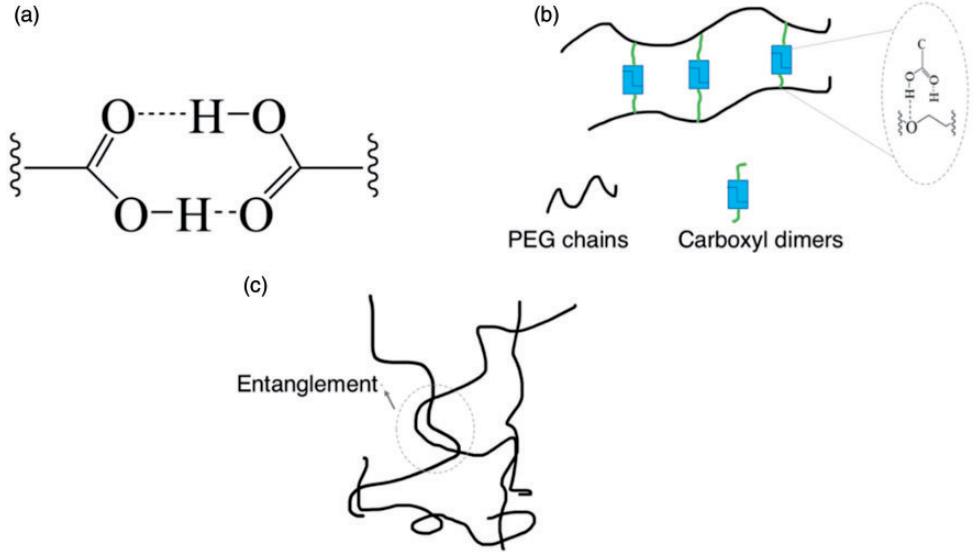

Figure 11. Two types of hydrogen bonding in PEG MDI DMPA. (a): hydrogen bonding between carboxylic acid, (b): hydrogen bonding between PEG and carboxyl group.[24] Schematic illustration (c) shows PEG chain crosses and gets entanglement that might occurred with increasing the molecular weight of PEG

bonds.[24] So, the changes that have been applied on the chemical state of the PEG molecule, e.g. increasing the number of oxyethylene (OE) groups in the PEG chain and therefore increasing the number of hydrogen-bondable groups, leads to a new mechanism to dissipate the strain energy.

Table 2 shows the linear relationship between the molecular weight of the PEG and young's modulus of the samples. The ultimate fracture force in PEG-1500-C is enhanced compared to the PEG-600-C, probably due to more interactions between the particles and the cement matrix.[43] As reported by E. McNamee et al., the higher molecular weight of PEG gives rise to the solid polymeric material, due to the entanglements of the PEG chains (Figure 10(c)).[44] Since the higher molecular weight of PEG leads to the higher strength of cement as well as inducing the new mechanism of energy dissipation, one can say that the polymer phase in the sample containing PEG-1500 is still enough flexible to bend/flex for contacting with the other surface. The point is that as the chain-length of PEG is increased, less energy is absorbed through the other processes (especially at higher level of strain (Figure 10)). Thus, there is a balance between the whole deformation (toughness) and the strength of samples with the increase of the PEG molecular weight.

Although this study was centered on the approaches that can be detected in FTIR curves, it is worth mentioning that there is one general mechanism due to adding the particles into the cement matrix. Admixtures produce some defects in cement matrixes, such as grain boundaries, dislocations and different interfaces. These defects can dissipate energy during vibration since defects and surfaces may slightly slip in relation to each other.[45,46] To get the desirable results following incorporation of particles, deep investigation of the factor affecting the particles distribution, ratio of particle to cement and different mixing process is essential.

In the whole process of mechanical tests, samples exchange energy with surrounding environment all the time. There is a conversion of the external mechanical energy into strain energy and the thermal energy is stored for its own internal energy. Meanwhile, the strain energy can be transformed to elastic energy, surface energy and so on, which will be released to the surrounding in the different forms such as acoustic emission and kinetic energy.[47] Consequently, energy change is always through the complete process of specimen's deformation and destruction which was detected in this study through the vibration of bonds.[27]

It is worth noticing that in the Portland cement, as the hydration proceeded, C-S-H gels, calcium hydroxide (CH) and ettringite (AFt) are anticipated to precipitate as the main hydrates.[14,31,48,49] In this study the volume of different phases in pure cement and the modified samples is not calculated. Therefore, the contribution of particles (SiO_2@polymer) on the formation of hydrates cannot be discussed in details, here. Sun et al. illustrated that there is a direct correlation between measured increasing compressive strength and hydrates volume.[14] The calculated fracture force of samples in Table 2 shows increasing trend as 8.46E-24, 5.18E-23 and 8.00E-23 (GPa mm^2) for the pure-cement, PEG-600-C and PEG-1500-C, respectively. Consequently, we can have several assumptions regarding the obtained values; (1) SiO_2@polymer particles might contribute to an increase in the total solid volume and a further reduction in porosity, (2) particles can function as fillers to fill the pore space or voids between cement particles. These interdependent effects probably lead to the denser microstructure, resulting in higher mechanical properties. However, still the question is open that if admixtures can change the hydration process of cement and would be an important subject for pursuing of this study.

Conclusion

In-situ FTIR results indicate how the particles in the cement matrix increase the mechanism of energy dissipation and prevent the complete release of strain energy, which leads to the sudden rupture of samples. In the pure cement, $Si-O-Si$ and $C-O$ bonds were mainly responsible for dissipating energy. Incorporating of particles reduce hydrolytic reaction energy of $Si-O-Si$, carrying more energy in the modified samples. Cement containing admixtures dissipated more energy with different mechanisms, as indicated by the presence of extra peaks associated with bending vibration of $O-Si-O$ and stretching of hydrogen bonds. From the un-modified sample to the cement with PEG-600 particles, both ultimate load of failure and deformation experienced same increasing trend. Enhancing the molecular weight of the PEG induce new process for energy absorption, stretching the $O-H$ bonds. Besides, PEG-1500-C show higher strength probably due to stronger interface bonding between particles and cement matrix. However, higher molecular weight of PEG decreased the overall deformation in this sample. Therefore, there is a balance between the strength and deformation of cements with the molecular weight of PEG.

In summary, since damping is the energy dissipation characteristic of material, it can be said that, according to the FTIR results, it is possible to evaluate the damping property of the samples subjected to external mechanical loading.

Declaration of Conflicting Interests

The author(s) declared no potential conflicts of interest with respect to the research, authorship, and/or publication of this article.

Funding

The author(s) disclosed receipt of the following financial sup port for the research, authorship, and/or publication of this article: The results presented in this paper have been gained within the DFG funded project TH 1566/3 2.

ORCID iD

Peter Thissen https://orcid.org/0000 0001 7072 4109

References

1. Zheng L, Huo XS and Yuan Y. Experimental investiga tion on dynamic properties of rubberized concrete. *Constr Build Mater* 2008; 22: 939 947.
2. Shalchy F and Rahbar N. Nanostructural characteristics and interfacial properties of polymer fibers in cement matrix. *ACS Appl Mater Interfaces* 2015; 7: 17278 17286.
3. Li W W, Ji W M, Liu Y, et al. Damping property of a cement based material containing carbon nanotube. *J Nanomater* 2015; 2015: 1 7.
4. Ou J. *Structural vibration control active, semi active and smart control systems*. China: Press of Science (in Chinese) 2003.
5. Han SJ and Chung DDL. Mechanical energy dissipation using carbon fiber polymer matrix structural composites with filler incorporation. *J Mater Sci* 2012; 47: 2434 2453.
6. Singh RK, Kant R, Pandey SS, et al. Passive vibration damping using polymer pads with microchannel arrays. *J Microelectromech Syst* 2013; 22: 695 707.
7. Sharafi S and Li GQ. Multiscale modeling of vibration damping response of shape memory polymer fibers. *Compos Part B Eng* 2016; 91: 306 314.
8. Geethamma V, Asaletha R, Kalarikkal N, et al. Vibration and sound damping in polymers. *Reson* 2014; 19: 821 833.
9. Constantinides G, Tweedie CA, Holbrook DM, et al. Quantifying deformation and energy dissipation of poly meric surfaces under localized impact. *Mater Sci Eng A Struct Mater Propert Microstruct Process* 2008; 489: 403 412.
10. Finegan IC and Gibson RF. Analytical modeling of damping at micromechanical level in polymer composites reinforced with coated fibers. *Compos Sci Technol* 2000; 60: 1077 1084.
11. Hu JL, Zhu Y, Huang HH, et al. Recent advances in shape memory polymers: structure, mechanism, func tionality, modeling and applications. *Progr Polym Sci* 2012; 37: 1720 1763.
12. Hager MD, Bode S, Weber C, et al. Shape memory poly mers: past, present and future developments. *Progr Polym Sci* 2015; 49 50: 3 33.
13. Song QJ, Chen HM, Zhou SB, et al. Thermo and pH sensitive shape memory polyurethane containing carbox yl groups. *Polym Chem* 2016; 7: 1739 1746.
14. Sun J, Cao X, Xu Z, et al. Contribution of core/shell TiO_2@ SiO_2 nanoparticles to the hydration of Portland cement. *Constr Build Mater* 2020; 233: 117127.
15. Hellstern H, Mamakhel A, Bremholm M, et al. Core shell nanoparticles by silica coating of metal oxides in a dual stage hydrothermal flow reactor. *Chem Commun* 2016; 52: 3434 3437.
16. Li S, Lin Q and Cui C. The effect of core shell particles on the mechanical performance of epoxy resins modified with hyperbranched polymers. *J Mater Res* 2016; 31: 1393 1402.
17. Gao J, Li J, Zhao S, et al. Effect of graft density and molecular weight on mechanical properties of rubbery block copolymer grafted SiO_2 nanoparticle toughened epoxy. *Polymer* 2013; 54: 3961 3973.
18. Jiang T, Kuila T, Kim NH, et al. Enhanced mechanical properties of silanized silica nanoparticle attached gra phene oxide/epoxy composites. *Compos Sci Technol* 2013; 79: 115 125.
19. Han B, Li Z, Zhang L, et al. Reactive powder concrete reinforced with nano SiO_2 coated TiO_2. *Constr Build Mater* 2017; 148: 104 112.
20. Theron C, Mokoena N and Ndwandwe OM. Solid state compound phase formation of TiSi2 thin films under stress. *S Afr J Sci* 2010; 105: 440 444.
21. Jaccodine RJ. Surface energy of germanium and silicon. *J Electrochem Soc* 1963; 110: 524 527.
22. Oliver WC and Pharr GM. An improved technique for determining hardness and elastic modulus using load and displacement sensing indentation experiments. *J Mater Res* 1992; 7: 1564 1583.
23. Oliver WC and Pharr GM. Measurement of hardness and elastic modulus by instrumented indentation: advances in understanding and refinements to methodology. *J Mater Res* 2004; 19: 3 20.
24. Zhu K, Song QJ, Chen HM, et al. Thermally assisted self healing polyurethane containing carboxyl groups. *J Appl Polym Sci* 2018; 135: 45929.
25. Oh T and Choi CK. Comparison between SiOC thin films fabricated by using plasma enhance chemical vapor depo sition and SiO_2 thin films by using Fourier transform infrared spectroscopy. *J Korean Phy Soc* 2010; 56: 1150 1155.
26. Tian RH, Seitz O, Li M, et al. Infrared characterization of interfacial Si O bond formation on silanized flat SiO_2/ Si surfaces. *Langmuir* 2010; 26: 4563 4566.
27. Lu S, Xu JY, Bai EL, et al. Effect of particles with dif ferent mechanical properties on the energy dissipation properties of concrete. *Constr Build Mater* 2017; 144: 502 515.
28. Liu N and Chen B. Experimental study of the influence of EPS particle size on the mechanical properties of EPS lightweight concrete. *Constr Build Mater* 2014; 68: 227 232.
29. Kamrani S, Hübler D, Ghasemi A, et al. Enhanced strength and ductility in magnesium matrix composites

reinforced by a high volume fraction of nano and submi cron sized SiC particles produced by mechanical milling and hot extrusion. *Materials* 2019; 12: 3445.
30. Slipenyuk A, Kuprin V, Milman Y, et al. Properties of P/ M processed particle reinforced metal matrix composites specified by reinforcement concentration and matrix to reinforcement particle size ratio. *Acta Mater* 2006; 54: 157 166.
31. Mendoza O, Giraldo C, Camargo SS, et al. Structural and nano mechanical properties of calcium silicate hydrate (C S H) formed from alite hydration in the pres ence of sodium and potassium hydroxide. *Cement Concr Res* 2015; 74: 88 94.
32. Kunther W, Lothenbach B and Skibsted J. Influence of the Ca/Si ratio of the C S H phase on the interaction with sulfate ions and its impact on the ettringite crystallization pressure. *Cement Concr Res* 2015; 69: 37 49.
33. Lothenbach B and Nonat A. Calcium silicate hydrates: solid and liquid phase composition. *Cement Concr Res* 2015; 78: 57 70.
34. Zhou Y, Hou DS, Geng GQ, et al. Insights into the inter facial strengthening mechanisms of calcium silicate hydrate/polymer nanocomposites. *Phys Chem Chem Phys* 2018; 20: 8247 8266.
35. Hou DS, Zhao TJ, Ma HY, et al. Reactive molecular simulation on water confined in the nanopores of the calcium silicate hydrate gel: structure, reactivity, and mechanical properties. *J Phys Chem C* 2015; 119: 1346 1358.
36. Zhu T, Li J, Lin X, et al. Stress dependent molecular pathways of silica water reaction. *J Mech Physics Solids* 2005; 53: 1597 1623.
37. Giraudo N, Bergdolt S, Laye F, et al. Dehydration and dehydroxylation of C S H phases synthesized on silicon wafers. *Appl Surf Sci* 2018; 433: 589 595.
38. Giraudo N, Wohlgemuth J, Bergdolt S, et al. Passivation of hydrated cement. *ACS Sustain Chem Eng* 2018; 6: 727 737.
39. Giraudo N and Thissen P. Carbonation competing func tionalization on calcium silicate hydrates: investigation of four promising surface activation techniques. *ACS Sustain Chem Eng* 2016; 4: 3985 3994.
40. Funk A and Trettin HR. DFT study on the effect of water on the carbonation of portlandite. *Ind Eng Chem Res* 2013; 52: 2168 2173.
41. Janotka I, Madejová J, Števula L, et al. Behaviour of Ca (OH) 2 in the presence of the set styrene acrylate disper sion. *Cement Concr Res* 1996; 26: 1727 1735.
42. Sobolev K, Sanchez F, Vivian I, et al. The use of nano particle admixtures to improve the performance of con crete. In: *12th international conference on recent advances in concrete technology and sustainability issues*, Ottawa, October 2012. pp.455 469.
43. Chi L, Lu S and Yao Y. Damping additives used in cement matrix composites: a review. *Compos Part B Eng* 2019; 164: 26 36.
44. McNamee CE, Yamamoto S and Higashitani K. Effect of the physicochemical properties of poly (ethylene glycol) brushes on their binding to cells. *Biophys J* 2007; 93: 324 334.
45. Chung D. Structural composite materials tailored for damping. *J Alloys Compound* 2003; 355: 216 223.
46. Zou D, Liu T and Teng J. Improving the damping ability by the addition of nano SiO_2 to the concrete materials. In: *Second international conference on smart materials and nanotechnology in engineering*. Bellingham: International Society For Optics And Photonics, 2009, p.74933C.
47. Li WM and Xu JY. Impact characterization of basalt fiber reinforced geopolymeric concrete using a 100 mm diameter split Hopkinson pressure bar. *Mater Sci Eng A Struct Mater Propert Microstruct Process* 2009; 513 514: 145 153.
48. Nguyen M T, Wang Z, Rod KA, et al. Atomic origins of the Self Healing function in cement polymer composites. *ACS Appl Mater Interfaces* 2018; 10: 3011 3019.
49. Izadifar M, Koniger F, Gerdes A, et al. Correlation between composition and mechanical properties of calci um silicate hydrates identified by infrared spectroscopy and density functional theory. *J Phys Chem C* 2019; 123: 10868 10873.